Available online at www.sciencedirect.com
SCIENCE DIRECT®
Thermochimica Acta 414 (2004) 137–143
thermochimica acta
www.elsevier.com/locate/tca

Nanocrystallization of anatase in amorphous TiO_2

Daniel Švadlák [a], Jana Shánělová [a], Jiří Málek [a,*], Luis A. Pérez-Maqueda [b], José Manuel Criado [b], Takefumi Mitsuhashi [c]

[a] *Department of Physical Chemistry, Faculty of Chemical Technology, University of Pardubice, Čs. Legií Sq. 565, 532 10 Pardubice, Czech Republic*
[b] *Instituto de Ciencia de Materiales de Sevilla, CSIC-UNSE, Americo Vespucio s/n, Isla de la Cartuja, Sevilla 41010, Spain*
[c] *Advanced Materials Laboratory, National Institute for Materials Science, 1-1 Namiki, Tsukuba-shi, Ibaraki 305-0044, Japan*

Received 4 September 2003; received in revised form 12 December 2003; accepted 15 December 2003

Abstract

The kinetics of nanocrystallization in amorphous TiO_2 has been studied in non-isothermal conditions by DSC. It was found that this process could be well described by standard Johnson–Mehl–Avrami–Kolmogorov (JMA) model with kinetic exponent $m \cong 1$. The kinetic parameters were calculated by simultaneous analysis of experimental data taken at different heating rates. These parameters were used as a basis for prediction of crystallization kinetics in isothermal conditions. The agreement between the JMA model prediction and experimental data depends on the method of preparation of amorphous TiO_2.

Keywords: Amorphous TiO_2; Crystallization; JMA model; Kinetic analysis

1. Introduction

Titania (TiO_2) is a material widely used in the electronics, ceramics and pigment industries. The high photocatalytic activity of titania has been well-documented [1]. It is also well known that such activity of amorphous titania is negligible and that of nanocrystalline anatase is greater rather that the rutile or brookite [2]. Many approaches have been used to obtain a nanocrystalline titania with desired properties. One of the most popular method is a controlled crystallization of amorphous titania (a-TiO_2) prepared by hydrolysis of alkoxide based sol–gel synthesis or precipitation process.

Exarhos and Aloi [3] studied isothermally the kinetics of the crystallization of a-TiO_2 films using in situ time-resolved Raman spectroscopy. They found that the JMA nucleation-growth model could describe the kinetics of this process. The JMA kinetic exponent extracted from experimental data was found to be $1.4 < m < 2$. Very similar behavior was reported also by Stojanović et al. [4] who found somewhat higher values of the kinetic exponent $2.2 < m < 3$ for crystallization of a-TiO_2 powder in non-isothermal conditions. Nevertheless, Zhang and Banfield [5] have found that the JMA model cannot describe the isothermal experimental data of crystal growth of nanocrystalline anatase in a-TiO_2, obtained by X-ray diffraction and transmission electron microscopy. They applied a kinetic model adopting Smoluchowski coagulation approach as a suitable tool to interpret quantitatively the experimental data. From their analysis it seems that the crystallization of amorphous titania is a complex process comprising several steps such as interface nucleation, crystal growth of anatase and oriented attachment of surrounding anatase particles.

The aim of this paper is to analyze the applicability of the JMA model for nanocrystallization process in amorphous titania using non-isothermal calorimetric measurements. The kinetic parameters are then calculated by simultaneous analysis of experimental data taken at different heating rates. The prediction capability of the kinetic models is tested by using isothermal crystallization data. The advantage of this approach is a possibility to reveal a complex crystallization behavior frequently found in oxide systems [6,7].

2. Experimental

Amorphous titania was prepared by controlled hydrolysis of titanium isopropoxide $Ti[OCH(CH_3)_2]_4$, supplied by WAKO Pure Chemical Industries, Ltd., by using two

* Corresponding author. Tel.: +420-466-036-554; fax: +420-466-036-361.
E-mail address: jiri.malek@upce.cz (J. Málek).

0040-6031/$ – see front matter © 2004 Elsevier B.V. All rights reserved.
doi:10.1016/j.tca.2003.12.009

different procedures. A stoichiometric amount of redistilled water was added dropwise to continuously stirred solution of titanium tetraisopropoxide at 25 °C. The precipitated white TiO_2 product was washed several times with redistilled water then filtered and dried at 120 °C for 90 min. The resultant partially dried powder sample was ground in an agate mortar and stored in a desiccator. This powder material has been labeled as sample A. Sample B was prepared by a dropwise adding of titanium tetraisopropoxide to a larger amount of stirred redistilled water at 25 °C. The precipitated powder was then treated in the same way as described above.

The prepared materials were characterized by X-ray diffraction analysis (XRD) using a Siemens Krystaloflex 4 diffractometer equipped with scintillation counter utilizing V-filtered Co radiation (30 kV, 20 mA). The scans were performed in the 2θ range of 7–50° at 0.05° steps for 4 s. The morphology of "as-prepared" and crystallized titania samples was examined by scanning electron microscopy (SEM) using a JEOL model JSM-5500LV microscope. The Brunauer–Emmett–Teller (BET) surface area was determined by a multiple point method, using a home-made nitrogen adsorption apparatus equipped with a TCD detector.

The behavior of partially dried samples was studied by thermogravimetry in air atmosphere at heating rate 5 K min^{-1} using a Sartorius balance BP210S coupled with programmed R.M.I. furnace model DX04T. The temperature programmed desorption (TPD) of species adsorbed at the sample surface was measured by a Balzers mass spectrometer OmniStar GSD 300 at 10 K min^{-1} in helium and also in oxygen atmosphere. The mass spectrometer was tuned to monitor following mass fragments *m*/*z*: 12 (C), 15 (CH_3–), 16 (O), 18 (H_2O), 27 (CH_3C–), 28 (CO; CH_3CH–), 32 (O_2) and 44 (CO_2).

The differential scanning calorimetry (DSC) measurements of crystallization kinetics under isothermal and non-isothermal conditions were performed by using a Perkin-Elmer Pyris 1 in an atmosphere of dry nitrogen. Samples of about 10 mg were encapsulated in aluminum sample pans. The instrument was previously calibrated with In and Zn standards.

3. Results

Fig. 1 shows a typical DSC and TG curves of both the samples A and B on heating at 5 K min^{-1} in a dry nitrogen atmosphere. In both cases, there is a broad endothermic effect in 80–210 °C range followed by the exothermic crystallization peak in 360–450 °C range. The endothermic effect can be associated mostly with the removal of water retained in partially dried powder. The corresponding weight loss at the onset of the crystallization peak is about −13.8% for sample A and −10.6% for sample B. The total weight loss at 500 °C is −14.1 and −10.9%, respectively. The TPD measurements confirmed that the endothermic effect corresponds to the water removal and partially also to the

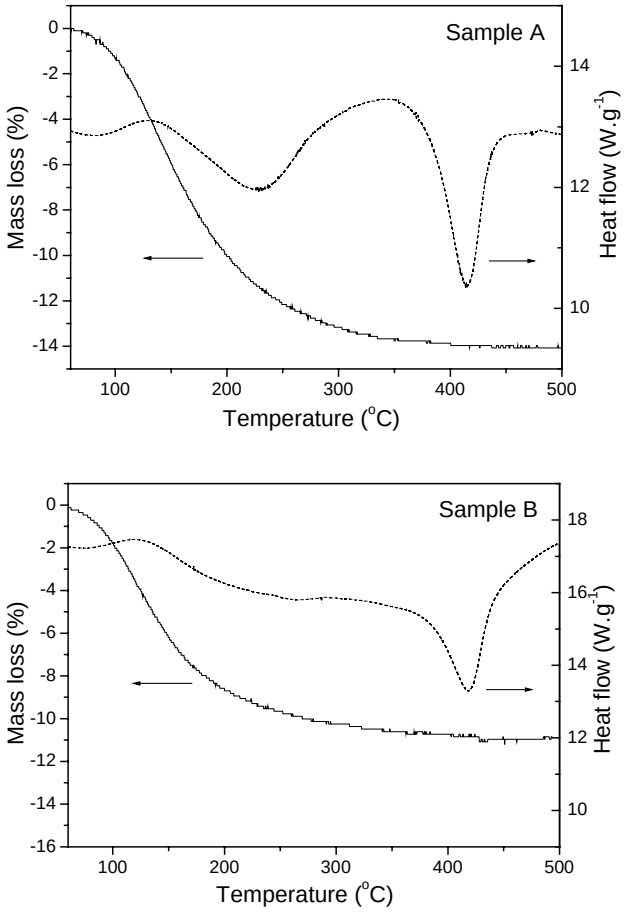

Fig. 1. DSC and TG curves for amorphous TiO_2 (samples A and B).

desorption of organic residues, that are present in the sample, as indicated also by carbon black color of the sample after DSC scan. These organic residues may strongly affect the crystallization behavior and, therefore, it is very important to remove them from the sample. It was found that the sample treatment at 250 °C in oxygen atmosphere for 1 h is sufficient for their successful removal and that the sample still retains its amorphous character. The samples A and B treated in this way were used for all following experiments.

Fig. 2 shows the non-isothermal crystallization data for the samples A and B (points) obtained by DSC measurements at heating rates $\beta = 5$, 10, 15 and 20 K min^{-1}. The crystallization peak maximum temperature T_p shifts with the heating rate for both samples. The value of activation energy E_a corresponding to the crystallization process can be derived by using the Kissinger's method [8] from the slope of $\ln(\beta/T_p^2)$ versus $1/T_p$ plot. It was found to be 276 ± 14 kJ mol^{-1} for sample A and 383 ± 30 kJ mol^{-1} for sample B.

Direct isothermal measurements of the crystallization kinetics of amorphous oxides prepared by hydrolysis is complicated by the fact that exothermic crystallization process is partially overlapped with the endothermic effect corresponding to the water (or other solvent) retained in these materials. Therefore, in order to obtain a reliable isothermal data the

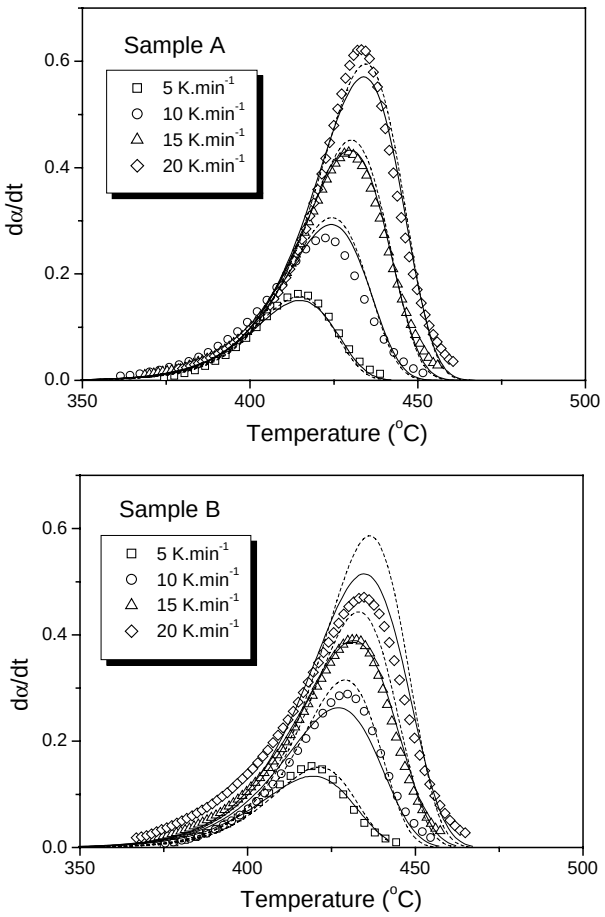

Fig. 2. Crystallization curves for amorphous TiO_2, recorded at different heating rates. The symbols are experimental DSC data evaluated from Eq. (2). The lines are JMA model predictions calculated by Eq. (5) for the kinetic parameters obtained by combined analysis (solid lines) and NPK method (broken lines). These parameters are given in Tables 3 and 4.

samples were isothermally annealed in the DSC calorimeter at 390 °C for various period of time, subsequently quenched to room temperature and then reheated at 10 K min^{-1}. The enthalpy change ΔH_c, corresponding to the area under the exothermal crystallization peaks of these annealed samples, is summarized in Table 1.

Table 1
The crystallization enthalpy of TiO_2 samples annealed at 390 °C

t (min)	$-\Delta H_c$ (J g^{-1})	
	Sample A	Sample B
0	133	116
2	105	96
5	79	94
8	–	62
10	63	54
20	52	11
30	26	13
45	9	–
60	0	0

Table 2
BET surface area for amorphous and crystalline samples of TiO_2

Sample	BET surface area (m^2 g^{-1})	
	Amorphous	Crystalline
A	277 ± 5	69 ± 3
B	276 ± 5	121 ± 1

The fraction crystallized during this isothermal annealing was estimated by using the following equation:

$$\alpha_c = \frac{\Delta H_c^\circ - \Delta H_c}{\Delta H_c^\circ} \quad (1)$$

where ΔH_c° is the crystallization enthalpy of amorphous sample without any annealing, i.e. ΔH_c ($t = 0$). This value found for sample A (Table 1) is similar to the crystallization enthalpy for a-TiO_2 reported previously (135 ± 15 J g^{-1}) [4].

The XRD patterns of as-prepared samples A and B exhibit very broad halo as typical for amorphous material. Clearly distinguished but still rather broad diffraction peaks were observed for fully crystallized TiO_2 samples, indicating a very fine crystallite size of anatase. An average size of these crystals estimated using the Scherrer formula [9], from the corrected half width of (1 0 1) difraction line, was found to be about 24 nm for sample A and 10 nm for sample B.

Amorphous sample shows typical morphology with well-separated grains of about 0.1 μm in size. A more complex structure consisting of agglomerate grains is seen for the fully crystallized sample. The grains are about 10 times larger than average crystallite size estimated from XRD line broadening. The results of BET multipoint surface area measurements for amorphous and crystalline samples of TiO_2 are summarized in Table 2.

4. Discussion

The analysis of non-isothermal DSC data is based on three assumptions. First, it is assumed that the crystallization rate dα/dt is proportional to the measured heat flow ϕ:

$$\left(\frac{d\alpha}{dt}\right) = \frac{\phi}{\Delta H_c^\circ}. \quad (2)$$

This assumption can be made for small samples and moderate heating rates provided that temperature and heat calibrations have been made properly. As ΔH_c° is a constant the crystallization rate can easily be calculated from heat flow versus temperature data. The fraction crystallized α is then obtained by partial integration of these data. Second assumption concerns the kinetic equation. For a solid state processes it can be expressed by a simple differential kinetic equation

$$\left(\frac{d\alpha}{dt}\right) = K(T) \cdot f(\alpha) \quad (3)$$

where $f(\alpha)$ is an algebraic expression of the kinetic model. These models have been developed for simplified geome-

try of the diffusion process, the reaction interface and its spatial movement or the nucleation-growth processes. The kinetic data for crystallization processes are usually interpreted in terms of the JMA model [10–12], i.e. $f(\alpha) = m(1-\alpha)[-\ln(1-\alpha)]^{1-1/m}$, where m is the kinetic exponent which is a function of the mechanism of crystallization process. Third assumption is related to this temperature dependence of the rate constant, expecting that it follows a simple Arrhenius form:

$$K(T) = A_a \exp\left(-\frac{E_a}{RT}\right) \tag{4}$$

where R is the gas constant, A_a the pre-exponential factor and E_a the apparent activation energy. The last two parameters should not depend on the temperature and the fractional conversion. Eqs. (3) and (4) then can be rearranged for the JMA model in the following form:

$$\left(\frac{d\alpha}{dt}\right) = A_a \exp\left(-\frac{E_a}{RT}\right) \cdot m(1-\alpha)[-\ln(1-\alpha)]^{1-1/m}. \tag{5}$$

Eq. (5) is most frequently used for the description of calorimetric crystallization data. Its validity in non-isothermal conditions is based on several additional assumptions [13] and, therefore, it should be thoroughly tested before being applied for the description of calorimetric data.

Probably the most popular testing method for isothermal data is based on the linearity of $\ln[-\ln(1-\alpha)]$ plot as a function of logarithm of time. A similar testing method has also been developed for non-isothermal data. It can be shown [14,15], that the dependence of $\ln[-\ln(1-\alpha)]$ as a function of reciprocal temperature should be linear for the JMA model, and the slope of this plot is expressed as

$$\frac{d\ln[-\ln(1-\alpha)]}{d(1/T)} \cong \frac{mE_a}{R}. \tag{6}$$

Fig. 3 shows these plots for the samples A and B at heating rate 10 K min^{-1}. The plots are practically linear in a wide temperature range, which suggests that the JMA model can be applied. The values of the kinetic exponent m estimated from Eq. (6) for the E_a obtained by Kissinger's method were found to be 1.01 ± 0.01 for sample A and 0.93 ± 0.01 for sample B.

An alternative test is based on the function defined as $z(\alpha) = f(\alpha)\int_0^\alpha [1/f(\alpha)]d\alpha$. The fraction crystallized at the maximum of the $z(\alpha)$ function can be obtained from the condition $[dz(\alpha)/d\alpha] = 0$. For the JMA model it should be close to 0.632 [6,7]. It has been shown [16] that the $z(\alpha)$ function can easily be obtained by a simple transformation of experimental data being proportional to the crystallization rate and T^2:

$$z(\alpha) \propto \left(\frac{d\alpha}{dt}\right) \cdot T^2. \tag{7}$$

Fig. 4 shows the $z(\alpha)$ plots for the samples A and B (points) transformed from experimental data shown in Fig. 2 by using Eq. (7). These plots are normalized within (0, 1) range to facilitate the comparison of different data sets. Overall shape of the $z(\alpha)$ plots seems to be invariant with

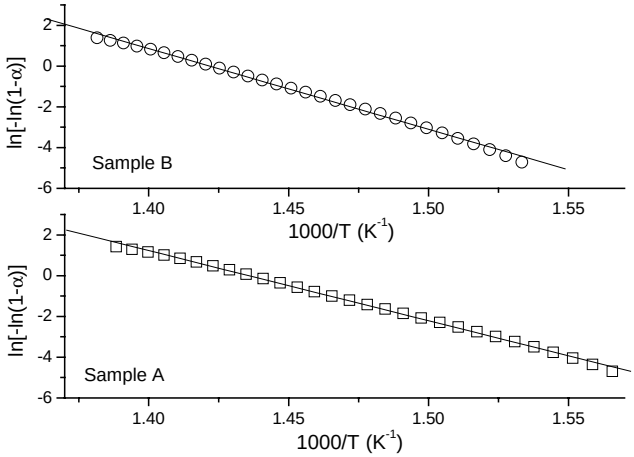

Fig. 3. The double logarithmic plot for non-isothermal crystallization data of the samples A and B measured at heating rate 10 K min^{-1}.

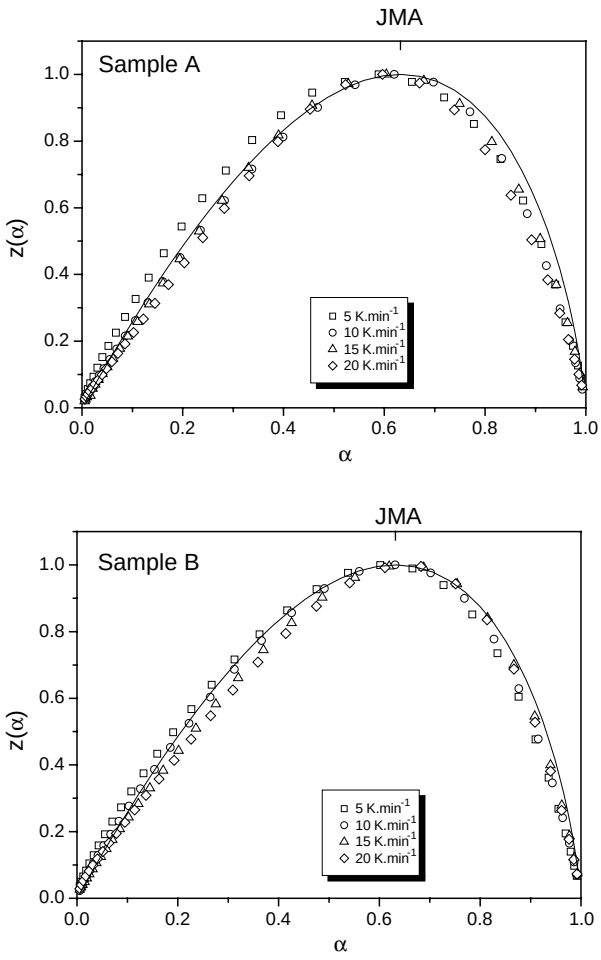

Fig. 4. Experimental data from Fig. 2 transformed by using Eq. (7) and normalized within (0, 1) interval (points). Solid lines correspond to the prediction of the JMA model.

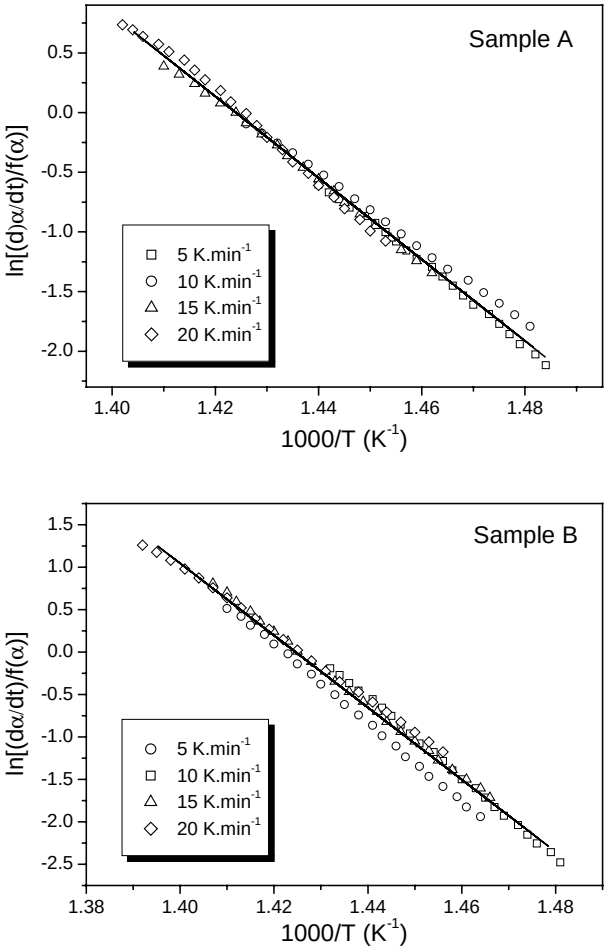

Fig. 5. Combined kinetic analysis of data shown in Fig. 2. Solid line corresponds to the linear regression fit.

respect to heating rate and well corresponds to the theoretically predicted dependence for the JMA model, i.e. $z(\alpha) \propto (1-\alpha)[-\ln(1-\alpha)]$, shown by solid line in Fig. 4. There is a well-defined maximum located at 0.61 ± 0.01 for sample A and 0.64 ± 0.01 for sample B. These values are in a reasonable agreement with the theoretical prediction. It seems, therefore, that this test also confirms the applicability of the JMA model for non-isothermal crystallization of anatase in amorphous TiO_2.

Recently, a new method of combined kinetic analysis has been introduced [17]. This method allows a simultaneous processing of crystallization data obtained under different experimental conditions and it is based on Eq. (5) rewritten in the following logarithmic form:

$$\ln\left[\frac{\mathrm{d}\alpha/\mathrm{d}t}{m(1-\alpha)[-\ln(1-\alpha)]^{1-1/m}}\right] = \ln A_\mathrm{a} - \left(\frac{E_\mathrm{a}}{RT}\right). \quad (8)$$

The plot of the left hand side of Eq. (8) versus the reciprocal of temperature yields a straight line for the correct value of the JMA kinetic exponent. This value is determined in the optimization procedure yielding to the best linear correlation corresponding to Eq. (8). Fig. 5 shows the result

Table 3
The kinetic parameters calculated by the combined kinetic analysis

Sample	m	E_a (kJ mol^{-1})	A_a (min^{-1})
A	1.19	284 ± 3	$(1.3 \pm 0.6) \times 10^{21}$
B	0.99	356 ± 6	$(3.5 \pm 2) \times 10^{26}$

of this combined kinetic analysis for the samples A and B. The optimization procedure yielded $m = 1.19$ for sample A and $m = 0.99$ for sample B. The slope and intercept of the straight line shown in Fig. 5 correspond to $-E_\mathrm{a}/R$ and $\ln A_\mathrm{a}$, respectively. These kinetic parameters are summarized in Table 3 for both samples of a-TiO_2.

One of the key steps in the kinetic analysis is the third assumption concerning the temperature dependence of the rate constant. Such assumption can be tested in so called non-parametric kinetic (NPK) method developed by Serra et al. [18,19]. In this method, the crystallization rate is discretized as a matrix whose rows correspond to different fractional conversion and whose columns correspond to different temperatures. The functions $f(\alpha)$ and $K(T)$ are discretized as column vectors, $\boldsymbol{f}$ and $\boldsymbol{k}$. The NPK method uses the singular value decomposition method to obtain both these vectors that contain the information about the kinetic model and allow to verify whether Arrhenius-type rate constant is applicable. Fig. 6 shows the elements of vector $\boldsymbol{k}$ plotted in logarithmic form as a function of reciprocal temperature. It is clearly seen that this plot follows Arrhenius-type dependence. The slope and intercept of the straight line shown in Fig. 6 correspond to $-E_\mathrm{a}/R$ and $\ln A_\mathrm{a}$, respectively. These kinetic parameters are summarized in Table 4 for both samples of a-TiO_2. The kinetic model can be determined from the plot of vector $\boldsymbol{f}$ as a function of fraction crystallized as shown in Fig. 6. This plot is practically linear in a wide range of α values indicating that the kinetic exponent is close to $m \cong 1$.

The values of kinetic parameters obtained by the NPK method are similar to those obtained by combined kinetic analysis. The kinetic exponent m is close to the value obtained from $\ln[-\ln(1-\alpha)]$ versus $1/T$ plot. The activation energy agrees within the combined error limits with the Kissinger's method estimation (see Section 3) for both samples A and B. It should be pointed out, however, that these results are about two times higher than the value reported by another authors [3–5]. The kinetic parameters summarized in Tables 3 and 4 can be used to calculate theoretical DSC curves for the JMA model. These theoretical DSC curves are compared with experimental data in Fig. 2. There is a fairly good agreement for sample A and also the difference between the NPK and combined kinetic analysis method are

Table 4
The kinetic parameters calculated by the NPK method

Sample	m	E_a (kJ mol^{-1})	A_a (min^{-1})
A	1.19	271 ± 4	$(1.4 \pm 1) \times 10^{20}$
B	0.93	359 ± 5	$(4.5 \pm 3) \times 10^{26}$

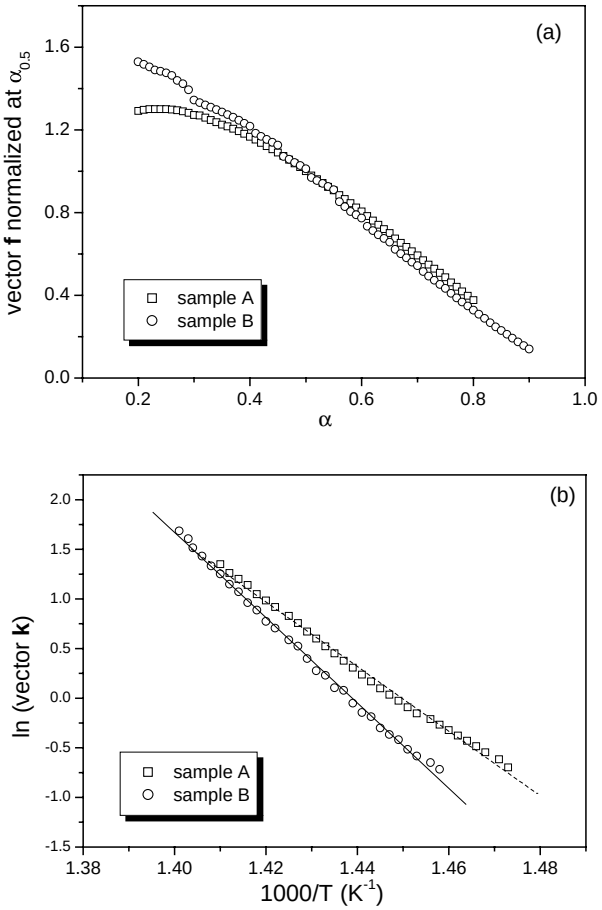

Fig. 6. NPK analysis of data shown in Fig. 2. (a) The elements of the vector $\boldsymbol{f}$ (normalized at $\alpha = 0.5$) plotted as a function of fraction crystallized. (b) The elements of the vector $\boldsymbol{k}$ plotted in logarithmic form as a function of reciprocal temperature.

relatively small. Considerably higher differences are found for sample B indicating that the crystallization process probably has a more complex nature than implicitly assumed in the JMA model.

It is interesting to analyze the fraction crystallized during isothermal annealing estimated by Eq. (1) from data shown in Table 1 (treated at $T = 390\,^{\circ}\mathrm{C}$). As mentioned above one of the most popular testing method for isothermal data is based on the linearity of $\ln[-\ln(1-\alpha)]$ plot as a function of logarithm of time. This plot shown in Fig. 7 reveals that isothermal data can be approximated by a linear dependence. The value of kinetic exponent determined from the slope of this dependence is not so reliable as there is a considerable scatter in experimental data: $m = 0.8 \pm 0.2$ (sample A), $m = 1.0 \pm 0.2$ (sample B). However, taking into account combined error limits, these parameters are in a reasonable agreement with the values obtained from non-isothermal data (see Tables 3 and 4) and they correspond approximately to the first-order process $m \cong 1$. Similar behavior has been observed in the final stage of nanocrystallization of amorphous ZrO_2 [6].

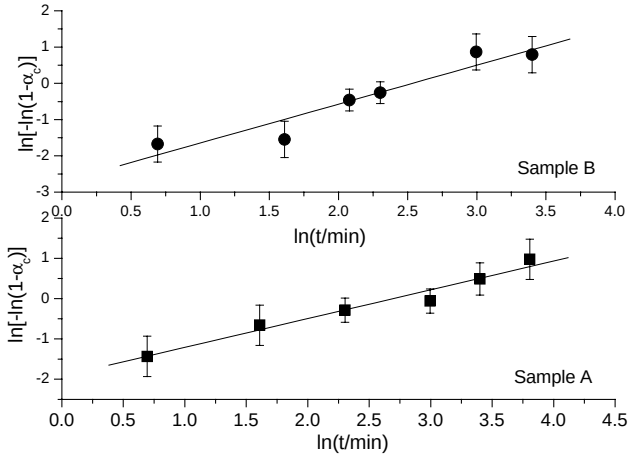

Fig. 7. The double logarithmic plot for isothermal crystallization data of the samples A and B (Table 1).

A convenient test of the kinetic model is based on comparison of independently obtained isothermal data and calculated isothermal curve based on the kinetic parameters extracted from non-isothermal experiments. The isothermal crystallization curve is expressed by the equation obtained by integration of Eq. (5):

$$\alpha_c = 1 - \exp\left\{-\left[t \cdot A_a \exp\left(-\frac{E_a}{RT}\right)\right]^m\right\}. \quad (9)$$

Fig. 8 shows isothermal curves calculated for kinetic parameters given in Table 3 (solid lines), Table 4 (broken lines) compared with the experimental values of α_c (points) for the samples A and B. There is a reasonably good agreement between experimental data and the prediction of the JMA model for sample A. Moreover, there is a negligible difference between the prediction based on the kinetic parameters given in Tables 3 and 4. This suggests that the JMA model is capable to describe well the crystallization extent in sample A under both isothermal and non-isothermal conditions (Fig. 8).

However, the same prediction for sample B largely underestimates isothermal data for $\alpha > 0.3$ range. Such differences in isothermal and non-isothermal kinetics in this sample clearly indicate that underlying crystallization mechanism might be complex. It should also be pointed out that the average size of nanocrystals formed during the crystallization process is about two times smaller than that for sample A. Similar factor can be found between the surface area ratio of amorphous and crystalline samples. Sample B also exhibits about 3.2% lower mass loss at the onset of the crystallization process, probably due to lower residual water content. These differences clearly indicate that the method of preparation of a-TiO_2 is essential for the crystallization behavior. The kinetic model is considered to be consistent if it provides a reliable description of both isothermal and non-isothermal data. From this point of view it can be concluded that only sample A can be described consistently by the JMA model.

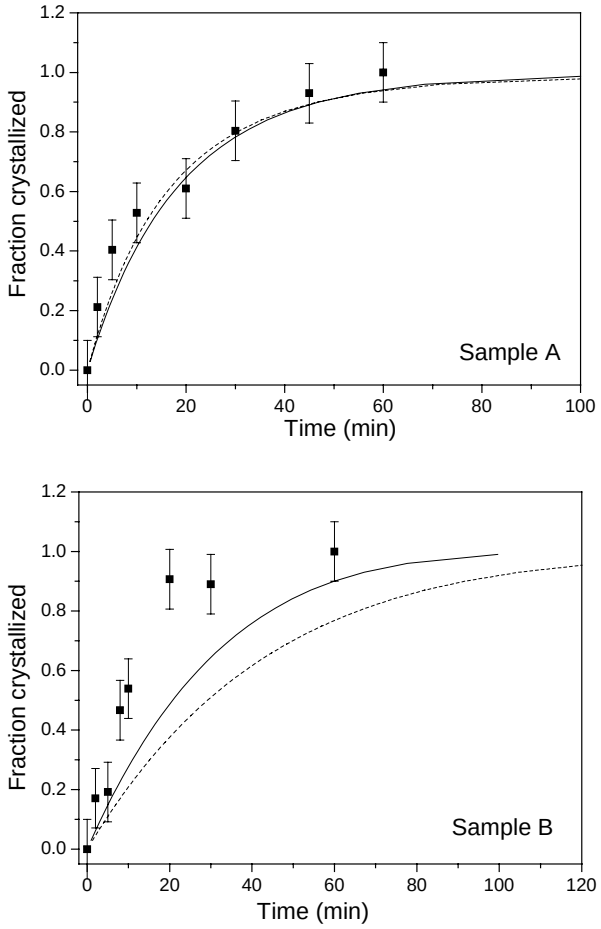

Fig. 8. Time evolution of fraction crystallized of amorphous TiO_2 at 390 °C. Points correspond to experimental data (Table 1). The curves are the JMA model prediction calculated by using Eq. (9) for the kinetic parameters given in Table 3 (solid lines) and Table 4 (broken lines).

Acknowledgements

This work was supported by the Cross-over research project on nuclear energy, promoted by MEXT, Japan.

References

[1] M.A. Fox, M.T. Dulay, Chem. Rev. 93 (1993) 341.
[2] B. Ohtani, Y. Ogawa, S. Nishimoto, J. Phys. Chem. B 101 (1997) 3746.
[3] G.J. Exarhos, M. Aloi, Thin Sol. Films 193/194 (1990) 42.
[4] B.D. Stojanović, Z.V. Marinković, G.O. Branković, E. Fidančevska, J. Therm. Anal. Cal. 60 (2000) 595.
[5] H. Zhang, J.F. Banfield, Chem. Mater. 14 (2002) 4145.
[6] J. Málek, T. Mitsuhashi, J. Ramírez-Castellanos, Y. Matsui, J. Mater. Res. 14 (1999) 1834.
[7] J. Málek, T. Mitsuhashi, J.M. Criado, J. Mater. Res. 16 (2001) 1862.
[8] H.E. Kissinger, Anal. Chem. 29 (1957) 1702.
[9] H.P. Klug, L.E. Alexander, X-ray Diffraction Procedures, John Wiley & Sons, New York, 1954 (Chapter 9).
[10] W.A. Johnson, R.F. Mehl, Trans. Am. Inst. Miner. Eng. 135 (1939) 419.
[11] M. Avrami, J. Phys. Chem. 8 (1940) 212.
[12] A.N. Kolmogorov, Izvestia Akad. Nauk USSR Ser. Math. 1 (1937) 355.
[13] D.W. Henderson, J. Non-Cryst. Sol. 30 (1979) 301.
[14] J. Šesták, Thermophysical Properties of Solids, Their Measurements and Theoretical Analysis, Elsevier, Amsterdam, 1984 (Chapters 8 and 9).
[15] J. Málek, Thermochim. Acta 355 (2000) 239.
[16] J. Málek, Thermochim. Acta 267 (1995) 61.
[17] L.A. Pérez-Maqueda, J.M. Criado, J. Málek, J. Non-Cryst. Sol. 320 (2003) 84.
[18] R. Serra, J. Sempere, R. Nomen, Thermochim. Acta 316 (1998) 37.
[19] R. Serra, J. Sempere, R. Nomen, J. Therm. Anal. Cal. 52 (1998) 933.